Density functional calculations of nuclear quadrupole coupling constants in the zero-order regular approximation for relativistic effects

Erik van Lenthe and Evert Jan Baerends
Afdeling Theoretische Chemie, Vrije Universiteit, De Boelelaan 1083, 1081 HV Amsterdam, The Netherlands

(Received 29 November 1999; accepted 10 February 2000)

The zeroth-order regular approximation (ZORA) is used for the evaluation of the electric field gradient, and hence nuclear quadrupole coupling constants, in some closed shell molecules. It is shown that for valence orbitals the ZORA-4 electron density, which includes a small component density (''picture-change correction''), very accurately agrees with the Dirac electron density. For hydrogen-like atoms exact relations between the ZORA-4 and Dirac formalism are given for the calculation of the electric field gradient. Density functional (DFT) calculations of the electric field gradients for a number of diatomic halides at the halogen nuclei Cl, Br, and I and at the metallic nuclei Al, Ga, In, Th, Cu, and Ag are presented. Scalar relativistic effects, spin–orbit effects, and the effects of picture-change correction, which introduces the small component density, are discussed. The results for the thallium halides show a large effect of spin–orbit coupling. Our ZORA-4 DFT calculations suggest adjustment of some of the nuclear quadrupole moments to $Q(^{79}\mathrm{Br}) = 0.30(1)$ barn, $Q(^{127}\mathrm{I}) = -0.69(3)$ barn, and $Q(^{115}\mathrm{In}) = 0.74(3)$ barn, which should be checked by future highly correlated *ab initio* relativistic calculations. In the copper and silver halides the results with the used gradient corrected density functional are not in good agreement with experiment. © *2000 American Institute of Physics.* [S0021-9606(00)30517-7]

I. INTRODUCTION

In a recent article[1] the zeroth-order regular approximation (ZORA)[2–5] to the Dirac equation was used for the calculation of the magnetic dipole hyperfine interaction, which is the interaction between the (effective) electronic spin of a paramagnetic molecule of interest and a magnetic nucleus in the molecule. In this article we will consider the electric quadrupole hyperfine interaction, which is the electrostatic interaction between an electric quadrupole of a nucleus and all other charges in the compound. This interaction can lead to splitting of lines in spectroscopic studies and the measured splittings are often reported as the nuclear quadrupole coupling constants (NQCC). Such a NQCC, which can be measured for example with microwave and nuclear quadrupole resonance spectroscopy, is proportional to the electric field gradient (EFG) at the nucleus and the electric nuclear quadrupole moment (NQM) of that nucleus. The EFG, which gives valuable information about the electron distribution surrounding the nucleus, is the property that we will calculate in this article.

One of the most accurate ways to determine the NQM of a certain nucleus is to combine the calculation of the EFG at that nucleus with the measured NQCC.[6] Highly correlated *ab initio* calculations can give accurate EFGs for open shell atoms or small closed shell molecules, see for example Refs. 7–12. In these references relativistic effects in the molecules were often approximated with the Douglas–Kroll–Hess Hamiltonian.[13,14] Fully relativistic all-electron (correlated) *ab initio* calculations of EFGs start to appear,[15,16] but they are still computationally demanding even for small molecules if they contain heavy elements.

An alternative to *ab initio* calculations is the use of density functional theory (DFT), since for many properties it can provide accurate results at a low computational cost. In Ref. 17, for example, results of scalar relativistic DFT calculations of the EFG at iron in various solids were compared with Mössbauer spectroscopic data for the NQCC to obtain the NQM of ^{57}Fe. On the other hand, recently Schwerdtfeger *et al.*[18] questioned the use of DFT for the calculation of EFGs in transition metal compounds, since they found a poor performance of many of the presently used functionals for the Cu EFG in CuCl. We will test one of those functionals in our calculations on a number of closed shell diatomic molecules. We use the (nonrelativistic) local density functional (LDA) with gradient correction (GGC) terms added, namely the Becke correction for exchange (Becke88),[19] and the Perdew correction for correlation.[20]

Recently DFT was also used for the calculation of the EFG at iron in some iron porphyrins and other molecules in Refs. 21, 22, for a comparison with Mössbauer spectroscopic data, and in Ref. 23, nonrelativistic DFT calculations were performed of the EFG at iodine in some iodine compounds. In fact there are many articles with results of nonrelativistic DFT and nonrelativistic *ab initio* calculations of EFGs in molecules, but only few with results from fully relativistic calculations.

An alternative to such fully relativistic calculations in molecules can be the use of approximate relativistic methods, like the mentioned Douglas–Kroll–Hess method or the ZORA method, which is used in this article. These are both two-component relativistic methods, for which it is important to include picture-change effects when evaluating expec-

tation values.[24,25] We will discuss such effects in the ZORA case. It will be demonstrated that the proper evaluation of the EFG in the ZORA method requires the introduction of the density from the small components, leading to what we call the ZORA-4 density. The precise relation of the use of the ZORA-4 density with the picture-change correction to order c^{-2} will be explicitly discussed.

Several other technical aspects of the calculation of EFGs will also be considered. In view of the heavy weighting of the near-nuclear region by the EFG operator, due to its $1/r^3$ behavior, polarization of the core, even if only slightly, may lead to nonnegligible effects. The possibility of a frozen core treatment therefore needs to be investigated. A related issue is the quality of the basis sets that are required, in particular in the core region. It should be possible to describe the core-orthogonality wiggles of the valence orbitals accurately with the basis set used. We will also discuss separately the scalar relativistic and spin–orbit effects on the calculated EFGs.

We calculate the EFG at the position of the halogen nuclei in the hydrogen halides, the interhalogens and in some metal halides, where the metals are aluminum, gallium, indium, thallium, copper, and silver. For these diatomic halides we also calculated the EFG at aluminum, gallium, and indium. Some of these molecules were also discussed in recent reviews by Palmer *et al.*[26–28] on experimentally observed halogen nuclear quadrupole coupling constants and *ab initio* calculations on a whole range of molecules.

II. THE ZORA EQUATION AND ELECTROSTATIC PERTURBATION

If only a time-independent electric field is present, the one-electron Dirac Kohn–Sham equations can be written in atomic units ($\boldsymbol{p}=-i\boldsymbol{\nabla}$), as an equation for the large component which after elimination of the small component (esc), reads

$$H^{\mathrm{esc}}\phi_i^D=\left(V+\boldsymbol{\sigma}\cdot\boldsymbol{p}\frac{c^2}{2c^2+\epsilon_i^D-V}\boldsymbol{\sigma}\cdot\boldsymbol{p}\right)\phi_i^D=\epsilon_i^D\phi_i^D, \quad (1)$$

and a companion equation which generates the small component from the large component

$$\chi_i^D=\frac{c}{2c^2+\epsilon_i^D-V}\boldsymbol{\sigma}\cdot\boldsymbol{p}\phi_i^D. \quad (2)$$

The normalization is such that the four-component Dirac electron density ρ_i^D,

$$\rho_i^D=(\phi_i^D)^\dagger\phi_i^D+\frac{c^2}{(2c^2+\epsilon_i^D-V)^2}(\boldsymbol{\sigma}\cdot\boldsymbol{p}\phi_i^D)^\dagger\boldsymbol{\sigma}\cdot\boldsymbol{p}\phi_i^D, \quad (3)$$

integrates to 1. In cases where spin–orbit (SO) coupling is not important one can use the scalar relativistic (SR) equation suggested in Refs. 29, 30,

$$H^{\mathrm{SR}}\phi_i^{\mathrm{SR}}=\left(V+\boldsymbol{p}\cdot\frac{c^2}{2c^2+\epsilon_i^{\mathrm{SR}}-V}\boldsymbol{p}\right)\phi_i^D=\epsilon_i^{\mathrm{SR}}\phi_i^{\mathrm{SR}}, \quad (4)$$

with the normalized electron density ρ_i^{SR} defined as

$$\rho_i^{\mathrm{SR}}=(\phi_i^{\mathrm{SR}})^\dagger\phi_i^{\mathrm{SR}}+\frac{c^2}{(2c^2+\epsilon_i^{\mathrm{SR}}-V)^2}(\boldsymbol{p}\phi_i^{\mathrm{SR}})^\dagger\cdot\boldsymbol{p}\phi_i^{\mathrm{SR}}. \quad (5)$$

This is not the only possible scalar relativistic equation, as was discussed in Ref. 31, where several scalar relativistic equations are compared.

The (SR) ZORA equation is the zeroth-order of the regular expansion of the (SR) relativistic equation,

$$H_{\mathrm{SR}}^{\mathrm{ZORA}}\Psi_i=(V+T[V])\Psi_i=\epsilon_i\Psi_i, \quad (6)$$

with

$$T^{\mathrm{ZORA}}[V]=\boldsymbol{\sigma}\cdot\boldsymbol{p}\frac{c^2}{2c^2-V}\boldsymbol{\sigma}\cdot\boldsymbol{p}$$

$$=\boldsymbol{p}\cdot\frac{c^2}{2c^2-V}\boldsymbol{p}+\frac{c^2}{(2c^2-V)^2}\boldsymbol{\sigma}\cdot(\boldsymbol{\nabla}V\times\boldsymbol{p}), \quad (7a)$$

$$T_{\mathrm{SR}}^{\mathrm{ZORA}}[V]=\boldsymbol{p}\cdot\frac{c^2}{2c^2-V}\boldsymbol{p}. \quad (7b)$$

The effective molecular Kohn–Sham potential V used in our calculations is the sum of the nuclear potential, the Coulomb potential due to the total electron density and the exchange-correlation potential, for which we will use nonrelativistic approximations. The ZORA kinetic energy operator T^{ZORA} depends on the molecular Kohn–Sham potential. The scalar relativistic (SR) ZORA kinetic energy operator $T_{\mathrm{SR}}^{\mathrm{ZORA}}$ is the ZORA kinetic energy operator without spin–orbit coupling. For convenience we will refer to the (SR) ZORA kinetic energy as $T_{(\mathrm{SR})}[V]$.

An improved one-electron energy can be obtained by using the scaled ZORA energy expression[32]

$$\epsilon_i^{\mathrm{scaled}}=\frac{\epsilon_i}{1+\langle\Psi_i|Q[V]|\Psi_i\rangle}, \quad (8)$$

with

$$Q^{\mathrm{ZORA}}[V]=\boldsymbol{\sigma}\cdot\boldsymbol{p}\frac{c^2}{(2c^2-V)^2}\boldsymbol{\sigma}\cdot\boldsymbol{p}, \quad (9a)$$

$$Q_{\mathrm{SR}}^{\mathrm{ZORA}}[V]=\boldsymbol{p}\cdot\frac{c^2}{(2c^2-V)^2}\boldsymbol{p}. \quad (9b)$$

The scaled ZORA method is the basis of (bond) energy evaluations, since it remedies the gauge dependency problem of the unscaled ZORA method, see the discussion in Ref. 32.

Let us now consider the effect of a small electric field described by the perturbing potential $V'(\boldsymbol{r})$, such as the potential due to a nuclear quadrupole. It is not possible to write the first-order perturbation energy simply as

$$\epsilon_i^{(1)}\approx\int\rho_i^Z V'd\boldsymbol{r}, \quad (10)$$

where ρ_i^Z is the ZORA density defined as

$$\rho_i^Z(\boldsymbol{r})=\Psi_i^\dagger(\boldsymbol{r})\Psi_i(\boldsymbol{r}). \quad (11)$$

The reason is that the ZORA wave functions $\Psi_i(\boldsymbol{r})$ are approximations to the relativistic two-component wave functions that result after a Foldy–Wouthuysen transformation U of the Dirac Hamiltonian and wave functions, $\Psi_i(\boldsymbol{r})$

$\approx \Psi_i^{\mathrm{FW}}(\boldsymbol{r}) = U\Psi^D(\boldsymbol{r})$. The Dirac electron density that ought to be integrated against V' is therefore $\rho_i^D(\boldsymbol{r}) = (U^\dagger\Psi_i(\boldsymbol{r}))^\dagger(U^\dagger\Psi_i(\boldsymbol{r}))$ rather than $\rho_i^Z(\boldsymbol{r})$. The effect of $U^\dagger$ is the introduction of small components as well as adding a first order (in c^{-2}) correction to the ''large component'' Ψ_i, cf. Ref. 24. We will discuss in the next section in more detail the effect of the picture-change U to order c^{-2}. The ZORA approach itself, however, does not follow a strict separation of the relativistic effects in orders of c^{-2}, and we derive the ZORA expression for the perturbation energy by applying first-order perturbation theory using the ZORA method including the perturbation $\lambda V'$,

$$(V+\lambda V'+T'[V+\lambda V'])\Psi_i' = \epsilon_i'\Psi_i', \tag{12}$$

where we have introduced the perturbation parameter λ.

Equation (12) will be solved using ordinary perturbation theory,

$$\Psi_i' = \Psi_i + \lambda\Psi_i^{(1)} + \cdots, \tag{13}$$

$$\epsilon_i' = \epsilon_i + \lambda\epsilon_i^{(1)} + \cdots. \tag{14}$$

If we use that

$$\frac{c^2}{2c^2-V-\lambda V'} = \frac{c^2}{2c^2-V} + \lambda V'\frac{c^2}{(2c^2-V)^2} + O(\lambda^2), \tag{15}$$

it is not difficult to see that the first-order energy $\epsilon_i^{(1)}$ can be described as the interaction of the external potential V' with an unnormalized density,

$$\epsilon_i^{(1)} = \left.\frac{\partial\epsilon'}{\partial\lambda}\right|_{\lambda=0} = \int (\rho_i^Z+\rho_i^S)V'\,d\boldsymbol{r}. \tag{16}$$

Here ρ_i^S is an (unnormalized) small component density defined as

$$\rho_i^S = \frac{c^2}{(2c^2-V)^2}(\boldsymbol{\sigma}\cdot\boldsymbol{p}\Psi_i)^\dagger\boldsymbol{\sigma}\cdot\boldsymbol{p}\Psi_i, \tag{17a}$$

$$\rho_{\mathrm{SR}}^S = \frac{c^2}{(2c^2-V)^2}(\boldsymbol{p}\Psi_i)^\dagger\cdot\boldsymbol{p}\Psi_i. \tag{17b}$$

We note that a gauge dependency problem arises from the density $\rho_i^Z+\rho_i^S$ being unnormalized: if V' is a small constant potential Δ, the first-order one-electron energy $\epsilon_i^{(1)}$ is not exactly Δ. Again we have to invoke the scaled ZORA method to avoid gauge dependency problems. The scaled one-electron energy is

$$\epsilon_i'^{\,\mathrm{scaled}} = \frac{\epsilon_i'}{1+\langle\Psi_i'|Q[V+\lambda V']|\Psi_i'\rangle}, \tag{18}$$

for which we have to use a perturbation expansion in λ,

$$\epsilon_i'^{\,\mathrm{scaled}} = \epsilon_i^{\mathrm{scaled}} + \lambda\epsilon_i^{(1)\mathrm{scaled}} + \cdots. \tag{19}$$

Now the first-order scaled ZORA one-electron energy $\epsilon_i^{(1)\mathrm{scaled}}$ is, apart from some terms which are of order $O(c^{-4})$, equal to

$$\epsilon_i^{(1)\mathrm{scaled}} = \left.\frac{\partial\epsilon_i'^{\,\mathrm{scaled}}}{\partial\lambda}\right|_{\lambda=0} \approx \int \rho_i^{Z4}V'\,d\boldsymbol{r}, \tag{20}$$

which is the electrostatic interaction of the external potential V' with the normalized one-electron density ρ_i^{Z4}, which we call the ZORA-4 density and which is defined as

$$\rho_i^{Z4} = \frac{\rho_i^Z+\rho_i^S}{1+\langle\Psi_i|Q[V]|\Psi_i\rangle}. \tag{21}$$

Note that

$$\int \rho_i^S\,d\boldsymbol{r} = \langle\Psi_i|Q[V]|\Psi_i\rangle, \tag{22}$$

which means that if ρ_i^Z is normalized to one, then according to Eq. (21) also ρ_i^{Z4} is normalized to one. The fact that we can describe the interaction with a normalized electron density is desirable, and we will therefore completely discard the small $O(c^{-4})$ terms. If we take for V' a small constant potential Δ, the first-order scaled one-electron energy $\epsilon_i^{(1)\mathrm{scaled}}$ in this approximation is Δ, since ρ_i^{Z4} is normalized to one.

In conclusion we make two remarks. First, we have given a derivation of the ZORA EFG using the analytical derivative with respect to the perturbation. This is of course equivalent to taking the numerical derivative by explicitly calculating the energy for a few discrete values of the perturbation strength parameter λ. This procedure has been proposed by Pernpointner, Seth, and Schwerdtfeger[12] for the calculation of EFGs, employing a point-charge model for the nuclear quadrupole. It has been applied with standard quantum chemical methods for total energy calculations, such as CCSD(T), but also with the two-component Douglas–Kroll relativistic method.[9–12,25] Avoiding the erroneous direct use of the density of the two-component wave function by taking the derivative with respect to the energy is commonly denoted as taking into account the picture change that has occurred in going from the four-component Dirac to a two-component formalism. However, such a picture change correction does, to order c^{-2}, not only consist of introduction of small components, which is what we find taking the derivative amounts to, but also entails correction of the large component, see Ref. 24. We will detail in the next section the full effect of picture-change correction to order c^{-2}.

In the second place we note that one may simply consider the ZORA equation as an approximate equation for the Dirac large component, in which the energy in the denominator has been neglected with respect to $2c^2$, cf. Eqs. (1) and (6). One then naturally has to take into account the small components, which may again be approximated by neglecting the energy in the denominator in Eq. (2). One then never leaves the Dirac picture. It has been shown by Sadlej *et al.*[33] that this approximation to the Dirac equation arises as the first-order treatment (denoted CPD4) in a special perturbation scheme. Natural extensions of this approach consist of taking, after a ZORA self-consistent field calculation, the ZORA (or preferably the scaled ZORA) one-electron energy (instead of the exact Dirac energy) in these equations and performing a single diagonalization for each orbital to obtain an improved approximation to the Dirac solution, or even iterating this procedure to self-consistency to obtain a full Dirac solution.[33,34]

An accurate approximation to the scaled ZORA method for the calculation of molecular bond energies is the ZORA

electrostatic shift approximation (ESA), described in Ref. 32. The first-order electrostatic interaction energy $\epsilon_i^{(1)\mathrm{ESA}}$ in this method is

$$\epsilon_i^{(1)\mathrm{ESA}} = \int \rho_i^Z V' \, d\boldsymbol{r}. \tag{23}$$

This is exactly the electrostatic interaction of the normalized one-electron density ρ_i^Z, which was already defined in Eq. (11), with the external potential V'. If we take for V' a small constant potential Δ, the first-order one-electron energy is Δ, as it should be. The ZORA ESA method was derived for, and applied in cases where the external potential V' is close to a constant over the region of ρ_i^Z (specifically, electrostatic potential of neighboring atoms over an atomic core state). However, this approximation need not be accurate, as we will demonstrate, with external potentials which do not have this property, like for example an electric quadrupole field of a nucleus.

III. PICTURE-CHANGE EFFECTS

In two-component relativistic methods the calculation of a property like the field gradient using total energy derivatives does not entail a picture-change error while a simplistic calculation of the expectation value from the two-component wave functions would. This does not imply that the picture change effects are rigorously accounted for even to lowest order in c^{-2}. In order to obtain the picture-change effects fully to a certain order one needs the wave functions accurate to at least that order.[24] In this section we will obtain the full picture-change effect to order c^{-2} [rather $1/(2c^2-V)$] using the first-order regularly approximated (FORA) Hamiltonian,[35] which is

$$H_{(\mathrm{SR})}^{\mathrm{FORA}} = H_{(\mathrm{SR})}^{\mathrm{ZORA}} + H_{(\mathrm{SR})}^{1} = H_{(\mathrm{SR})}^{\mathrm{ZORA}} - \tfrac{1}{2} Q[V] H_{(\mathrm{SR})}^{\mathrm{ZORA}} - \tfrac{1}{2} H_{(\mathrm{SR})}^{\mathrm{ZORA}} Q[V]. \tag{24}$$

A different possibility is to use the closely related IORA (infinite-order regular approximated) Hamiltonian, see Ref. 36. The Hamiltonians and wave functions in this section may be taken to be scalar relativistic ones or to include SO coupling. The developments of this section apply in both cases. The FORA Hamiltonian is the Foldy–Wouthuysen[37] transformed Dirac Hamiltonian correct to order $1/(2c^2-V)$, which contains all terms to order c^{-2}, but also includes some higher-order terms. We will now use first-order perturbation theory, where we take as zeroth-order the ZORA equation with solution Ψ_i, to obtain expressions for Ψ_i^{FORA}, the Foldy–Wouthuysen transformed Dirac wave function correct to order $1/(2c^2-V)$. This allows us to obtain the FORA density. In order to establish the picture-change error we compare this density with the density obtained after a Foldy–Wouthuysen (FW) back transformation of Ψ_i^{FORA} to order $1/(2c^2-V)$. The FW transformation matrix to this order is available from Ref. 5. This FW back transformation will yield the Dirac large component, and generate the small component, both to the required order. We will denote these as ϕ_i^{DFORA} and χ_i^{DFORA}, respectively.

$$\begin{aligned}\Psi_i^{\mathrm{FORA}} &= \Psi_i + \sum_{k\neq i} \frac{\langle \Psi_k | H^1 | \Psi_i \rangle}{\epsilon_i - \epsilon_k} \Psi_k \\ &= \Psi_i - \frac{1}{2} \sum_{k\neq i} \frac{\epsilon_i + \epsilon_k}{\epsilon_i - \epsilon_k} \langle \Psi_k | Q[V] | \Psi_i \rangle \Psi_k \\ &= \left(1 - \frac{1}{2} \langle \Psi_i | Q[V] | \Psi_i \rangle \right) \Psi_i + \frac{1}{2} Q[V] \Psi_i \\ &\quad - \epsilon_i \sum_{k\neq i} \frac{\langle \Psi_k | Q[V] | \Psi_i \rangle}{\epsilon_i - \epsilon_k} \Psi_k .\end{aligned} \tag{25}$$

Here use has been made of the resolution of the identity

$$|\Psi_i\rangle\langle\Psi_i| + \sum_{k\neq i} |\Psi_k\rangle\langle\Psi_k| = 1. \tag{26}$$

The electron density in the Foldy–Wouthuysen (or Schrödinger) picture correct to order $1/(2c^2-V)$ is

$$\rho_i^{\mathrm{FW\ FORA}} = (\Psi_i^{\mathrm{FORA}})^\dagger \Psi_i^{\mathrm{FORA}} = (1 - \langle \Psi_i | Q[V] | \Psi_i \rangle) \rho_i^Z - \epsilon_i \sum_{k\neq i} \frac{\langle \Psi_k | Q[V] | \Psi_i \rangle \Psi_i^\dagger \Psi_k + \langle \Psi_i | Q[V] | \Psi_k \rangle \Psi_k^\dagger \Psi_i}{\epsilon_i - \epsilon_k} + \frac{1}{2} (Q[V] \Psi_i)^\dagger \Psi_i + \frac{1}{2} \Psi_i^\dagger Q[V] \Psi^i. \tag{27}$$

We now calculate the Dirac density to the same order by first obtaining the Dirac large and small components from the FW back transformation:

$$\phi_i^{\mathrm{DFORA}} = \Psi_i^{\mathrm{FORA}} - \frac{1}{2} Q[V] \Psi_i = \left(1 - \frac{1}{2} \langle \Psi_i | Q[V] | \Psi_i \rangle \right) \Psi_i - \epsilon_i \sum_{k\neq i} \frac{\langle \Psi_k | Q[V] | \Psi_i \rangle}{\epsilon_i - \epsilon_k} \Psi_k , \tag{28}$$

$$\chi_i^{\mathrm{DFORA}} = \frac{c}{2c^2 - V} \boldsymbol{\sigma} \cdot \mathbf{p} \Psi_i , \tag{29}$$

and then obtaining the density in the Dirac picture as

$$\rho_i^{\mathrm{DFORA}}=(\phi_i^{\mathrm{DFORA}})^\dagger\phi_i^{\mathrm{DFORA}}+(\chi_i^{\mathrm{DFORA}})^\dagger\chi_i^{\mathrm{DFORA}}$$
$$=(1-\langle\Psi_i|Q[V]|\Psi_i\rangle)\rho_i^Z-\epsilon_i\sum_{k\neq i}\frac{\langle\Psi_k|Q[V]|\Psi_i\rangle\Psi_i^\dagger\Psi_k+\langle\Psi_i|Q[V]|\Psi_k\rangle\Psi_k^\dagger\Psi_i}{\epsilon_i-\epsilon_k}+\rho_i^S, \tag{30}$$

with ρ_i^S defined in Eq. (17). Correct to the same order this can also be written as

$$\rho_i^{\mathrm{DFORA}}=\rho_i^{Z4}-e_i\sum_{k\neq i}\frac{\langle\Psi_k|Q[V]|\Psi_i\rangle\Psi_i^\dagger\Psi_k+\langle\Psi_i|Q[V]|\Psi_k\rangle\Psi_k^\dagger\Psi_i}{\epsilon_i-\epsilon_k}. \tag{31}$$

Thus the Dirac electron density is the ZORA-4 electron density ρ_i^{Z4} plus a correction term, which is first-order in $\epsilon_i/(2c^2-V)$. This means that the ZORA-4 density can very accurately agree with the Dirac density, especially for valence orbitals which have small energy eigenvalues.

Up to first-order in $1/(2c^2-V)$ the picture-change effects in the density can now be obtained from the difference between the FW (FORA) and Dirac (FORA) densities,

$$\rho_i^{\mathrm{FW\ FORA}}-\rho_i^{\mathrm{DFORA}}=\tfrac{1}{2}(Q[V]\Psi_i)^\dagger\Psi_i+\tfrac{1}{2}\Psi_i^\dagger Q[V]\Psi_i-\rho_i^S. \tag{32}$$

Thus the picture change effect is more than the effect of just adding a small component density, and then renormalize, see for this point also Ref. 24. In order to obtain the picture-change effect consistently to order $1/(2c^2-V)$, one has to calculate besides the small component density the terms

$$\frac{1}{2}(Q[V]\Psi_i)^\dagger\Psi_i+\frac{1}{2}\Psi_i^\dagger Q[V]\Psi_i=\frac{\epsilon_i-V}{2c^2-V}\rho_i^Z+O(c^{-4}). \tag{33}$$

This means that for the calculation of the picture-change effect, and for the calculation of the electron density in the Foldy–Wouthuysen (or Schrödinger) picture as well, we need to calculate terms which are of order $(\epsilon_i-V)/(2c^2-V)$, which can be important for the density close to a nucleus. However, our primary goal is not to calculate the picture change effects very accurately. We need to obtain the electron density (in the Dirac picture) to sufficient accuracy. In fact, if we use the ZORA-4 electron density ρ_i^{Z4}, which we have seen is consistent within the ZORA scheme, we have not fully accounted for picture-change effects to order c^{-2}, but we do have a very accurate approximation, especially for valence orbital densities, since the missing terms are of order $\epsilon_i/(2c^2-V)$, see Eq. (31). For the hydrogen-like atom we already know exactly how large these missing terms are (to all orders), since the exact relation between the ZORA eigenfunctions and the Dirac eigenfunctions is known.[35] In this case the missing terms are of order $\epsilon_i/2c^2$; see also next section.

IV. ELECTRIC FIELD GRADIENTS IN HYDROGEN-LIKE ATOMS

In Ref. 35 it has been shown for the hydrogenic one-electron atoms, that the ZORA eigenfunctions Ψ_i are proportional to scaled Dirac large component spinors ϕ_i^D

$$\Psi_i(\boldsymbol{r})=\frac{1}{\mu^2}\phi_i^D\left(\frac{\boldsymbol{r}}{\mu}\right), \tag{34}$$

where the scaling factor μ depends on the energy

$$\mu=\frac{2c^2+\epsilon_i^D}{2c^2}=\frac{2c^2}{2c^2-\epsilon_i}. \tag{35}$$

In this case the ZORA-4 electron density ρ_i^{Z4} and the Dirac electron density ρ_i^D are related as

$$\rho_i^{Z4}(\boldsymbol{r})=\frac{1}{\mu^3}\rho_i^D\left(\frac{\boldsymbol{r}}{\mu}\right). \tag{36}$$

Similar exact relations also exist between the SR ZORA equation and the SR Eq. (4).

For the calculation of the electric field gradient (EFG) at the origin we need to calculate matrix elements of

$$V'_{kl}=\frac{\delta_{kl}}{r^3}-3\frac{x_kx_l}{r^5}, \tag{37}$$

with x_k a Cartesian coordinate. In the case of a hydrogen-like atom it is not difficult to show that

$$\int\rho_i^DV'_{kl}\,d\boldsymbol{r}=\mu^3\int\rho_i^{Z4}V'_{kl}\,d\boldsymbol{r}, \tag{38}$$

where ρ_i^D is the Dirac electron density, ρ_i^{Z4} is the ZORA-4 electron density, and μ was given in Eq. (35). Application of this equation for Xe^{53+} gives that the EFG due to the ZORA-4 electron density of the $2p_{3/2}$ spinor for a given m_j-value is approximately 3% larger than the EFG due to the corresponding Dirac electron density. This difference reduces to 0.5% if we compare the EFGs due to the electron density of the $5p_{3/2}$ spinor. Note that for spherical electron densities the EFG at the origin is zero.

We can do the same exercise in the spin-free formalism, where SR ZORA (-4) results are compared with the results of the SR Eq. (4). In Table I the results are given for the numerically calculated EFGs (*zz*-component) due to a *p*-orbital with $m_l=0$. This table allows various comparisons. In the first place it is clear from Table I that introduction of the small component density (correcting for the picture-change error) is important: the ZORA density gives an approximate 6% deviation from the ZORA-4 density for all of the *p*-orbitals. In the second place we can see that the EFG due to the SR ZORA-4 electron density of the ''valence'' $5p$-orbital is approximately 0.5% larger than the exact EFG of the SR calculation. The difference increases to 3% if we compare the ZORA-4 and Dirac EFGs due to the electron

TABLE I. The electric field gradient (a.u) at the nucleus in the one-electron ion Xe^{+53} due to a p-orbital with $m_l=0$ as calculated with different spin-free models.

	NR[a]	SR	SR	SR	MVD[b]		DK[b]	
		ZORA[c]	ZORA-4[c]	Dirac[c,d]	No. P.C.[e]	P.C.[f]	No. P.C.[e]	P.C.[f]
$2p$	−5248.8	−6518.5	−6150.1	−5968.7	−6549.4	−5786.5	−6777.9	−5760.4
$3p$	−1552.2	−1963.0	−1835.6	−1811.5	−2010.9	−1742.6	−2100.0	−1734.9
$4p$	−656.1	−821.3	−773.3	−767.6	−856.1	−736.8	−896.1	−733.2
$5p$	−335.9	−419.6	−395.0	−393.1	−439.7	−377.0	−460.4	−375.0

[a]The exact nonrelativistic result is $-4Z^3/15n^3$.
[b]Values taken over from Ref. 25. MVD is the spin-free mass-velocity Darwin method and DK is the spin-free Douglas–Kroll method.
[c]This work.
[d]SR Dirac according to Eq. (4).
[e]No change of picture taken into account.
[f]Picture-change effects taken into account.

density of the $2p$-orbital. These findings numerically confirm the relation given in Eq. (38). Since the $5p$ orbital is in this highly charged ion of course at much lower energy and much more contracted than the real valence $5p$-orbital in the neutral Xe atom, we may conclude that the ZORA-4 error for valence orbitals will be very small. It will be larger for the deep core orbitals, but since the cores are spherical and will exhibit only small polarizations, the core contribution to the total EFG will probably be so small that the ca. 3% difference between ZORA-4 and SR Dirac EFGs for the deep core is unimportant. This point will be explicitly verified later. Table I also shows results of Kellö and Sadlej[25] of mass-velocity Darwin (MVD), and spin-free Douglas–Kroll (DK) calculations. They calculated the picture-change effects in the EFGs for these methods with the help of a finite nuclear quadrupole model. We note that in both cases but in particular in the Douglas–Kroll case the uncorrected EFGs are larger in an absolute sense (more negative) than the ZORA values. On the other hand the picture-change correction is so much larger (over 20% in most cases, i.e., more than two times larger than the differences between the ZORA and ZORA-4 results) that the corrected values are considerably smaller than the ZORA-4 values. They also differ more from the SR benchmark values and are smaller than these by 3%–5%, while the ZORA-4 values were 0.5%–3% larger (referring all the time to absolute values). Of course, the various two-component methods all yield approximations to the rigorous two-component Foldy–Wouthuysen solutions. They may not be expected to give identical answers. Moreover, as was discussed before, the results obtained by taking the energy derivative do not provide the complete picture-change effects, see Eq. (33). One also has to remember that there is not a unique spin-free Dirac equation,[31] and different spin-free Dirac equations will give different results, although it is at present unknown to what extent. For the SR ZORA equation it is convenient to compare with the conventional SR Eq. (4), since for hydrogen-like atoms there exist exact relations between the solutions of these equations.[35]

There is no ambiguity when making comparisons based on full ZORA and Dirac calculations, including SO coupling. Pyykkö and Seth[38] calculated the EFG due to an orbital which consists of an arbitrary combination of $p_{1/2}$ and $p_{3/2}$ Dirac spinors. The combination

$$\Psi_p^{\mathrm{QSR}} = -\sqrt{\tfrac{1}{3}}\,p_{1/2,1/2} + \sqrt{\tfrac{2}{3}}\,p_{3/2,1/2} \tag{39}$$

is of special interest, since in case the spin–orbit coupling has no effect (spatial parts of $p_{1/2}$ and $p_{3/2}$ equal) this orbital is a p-orbital with $m_l=0$ and spin α. In general we may denote the orbital of Eq. (39) as quasiscalar relativistic, QSR. The orbital in Eq. (39) is not an eigenfunction of the Hamiltonian including spin–orbit coupling, but a linear combination of such eigenfunctions. It can however serve as a model for the explanation of effects of spin–orbit coupling in molecular calculations, as was done by Pyykkö and Seth.[38] They showed that any other normalized combination of a $p_{1/2,1/2}$ and $p_{3/2,1/2}$ spinors than the QSR combination given in Eq. (39) will (almost always) lead to a lower EFG. For example, the EFG due to a pure $p_{3/2,1/2}$ spinor is less than one-half times the calculated EFG due to the QSR combination, and the EFG due to a pure $p_{1/2,1/2}$ spinor is zero. Here we use the QSR orbital for a comparison of ZORA and Dirac results. In Table II the results are given for the numerically calculated EFGs at the origin of the hydrogen-like atom Xe^{53+} due to the QSR p-orbital given in Eq. (39). These results can be compared with those given in Table I. The calculated EFGs of the QSR orbitals in Table II are only a few percent larger than the calculated EFGs of the SR orbitals in Table I. The conclusions drawn from Table I can be seen to hold basically unmodified for the QSR results. The effect of the small component in the ZORA calculations (difference between ZORA and ZORA-4 results in Table II) is ca. 4%, a little bit smaller than the 6% effect of the small component in the scalar relativistic ZORA calculations (dif-

TABLE II. The electric gradient (a.u.) at the nucleus in the one-electron ion Xe^{+53} due to the quasiscalar relativistic (QSR) combination of a $p_{1/2}$ and $p_{3/2}$ spinor as given in Eq. (39), which closely resembles a p-orbital with $m_l=0$ and spin α.

	QSR ZORA	QSR ZORA-4	QSR DIRAC
$2p$	−6641.1	−6366.5	−6178.9
$3p$	−1986.8	−1908.0	−1882.9
$4p$	−837.5	−804.8	−798.9
$5p$	−427.8	−411.3	−409.3

ference between SR ZORA and SR ZORA-4 results in Table I). [In the ZORA case the effect of the small component would be larger (smaller) if a normalized combination of $p_{1/2,1/2}$ and $p_{3/2,1/2}$ spinors would have relatively more (less) $p_{1/2,1/2}$ character than the QSR combination used here.] The difference between the ZORA-4 and the Dirac EFGs for the QSR orbitals is very similar to the SR case, the ZORA-4 EFGs being larger (in an absolute sense) by 0.5% for the $5p$ to 3% for the $2p$.

V. BASIS SET EFFECTS AND THE FROZEN CORE APPROXIMATION

In this section the effect of the basis set and the frozen core approximation on the calculated EFGs is investigated. We will first demonstrate some points using atomic calculations, and will then turn to molecular calculations. The ADF (Amsterdam density functional) program[39–41] is used for electronic structure calculations on molecular systems. The one-electron equations arising in the Kohn–Sham formulation of density functional theory, are solved by self-consistent field calculations. In the calculations a Slater-type orbital (STO) basis set is used. The ADF program can perform nonrelativistic and (SR) ZORA calculations.[32,42] We applied a numerical integration procedure[40] for the evaluation of the integrals needed for the calculation of the electric field gradient.

In the present calculations the same large basis sets are used as in Ref. 42. These all-electron basis sets are triple-ζ in the core and quadruple-ζ in the valence with at least three polarization functions added. The exponents of the STOs were fitted to numerical scalar relativistic ZORA orbitals. For the heavier atoms, these basis sets contain extra $1s$ and $2p$ STO functions, in order to describe the core orbitals accurately. In basis set *B* extra polarization functions were added. The size of the STO basis set *B* is $(5s3p3d1f)$ for H, $(9s5p3d3f)$ for F, $(12s8p4d4f)$ for Cl, $(15s11p7d4f)$ for Br, and $(18s14p9d4f)$ for I. Basis set *A* is basis set *B* plus one extra-tight $1s$ STO plus three extra-tight $2p$ STOs. Basis set *C* is the standard ADF ZORA all-electron basis set IV, which is double-ζ in the core and triple-ζ in the valence. The size of the STO basis set *C* is $(3s1p)$ for H, $(5s3p1d)$ for F, $(7s5p1d)$ for Cl, $(8s7p4d)$ for Br, and $(12s10p6d)$ for I. Basis set *D* is the same as basis set *C*, except that the core orbitals are kept frozen during the calculation. Separate SR ZORA atomic calculations were performed to generate these frozen core orbitals. Basis set *E* is the standard ADF SR ZORA frozen-core basis set IV, in which the basis set of the valence orbitals is the same as in basis set *C* or *D*. However, this basis set *E* only contains a single-ζ core description of the core wiggles of the valence orbitals, whereas in basis set *D* this is a double-ζ description. In the frozen core calculations the orbitals up to $(n-1)s$ and $(n-1)p$ were kept frozen, including the $3d$ for I.

Calculations on the EFG of the valence $5p$-electron of the neutral iodine atom, employing the simple $X\alpha$ approximation to the exchange-correlation potential with $\alpha=0.7$, are used to illustrate the effects of basis sets (Table III). The orbitals (spinors) of the open shell I atom were calculated in spin-restricted average-of-configuration calculation, where during the self-consistency cycles the electrons are distributed equally over the subspecies of the open shell irreps. For atoms this will ensure a spherical density. If spin–orbit coupling is present the electrons are divided in a spin–orbit averaged way over the different open shell irreps such that if the spin–orbit coupling is zero the occupation would be the same as in the scalar relativistic case. For the neutral iodine atom with a p^5 configuration this means that 5/3 of an electron is placed in the $p_{1/2}$ shell and 10/3 in the $p_{3/2}$ shell. The EFG is subsequently calculated for the QSR combination of a $5p_{1/2}$ and $5p_{3/2}$ spinor as given in Eq. (39).

TABLE III. Calculated EFGs due to a $5p$-orbital with $m_l=0$ (NR and SR ZORA case) or due to the combination of a $5p_{1/2}$ and $5p_{3/2}$ spinor as given in Eq. (39) (ZORA and DIRAC case) of the neutral iodine at the origin spin restricted $X\alpha(\alpha=0.7)$ calculations. The numerically calculated values are given in a.u.; the basis set results are given in percent difference with respect to the numerical value. The basis sets are described in the text. Columns *D* and *E* refer to frozen core calculations.

		Basis set error (%)				
	Numerical (a.u.)	*A*	*B*	*C*	*D*	*E*
NR	−13.509	0.0	0.0	0.2		
SR ZORA	−16.002	0.0	−0.6	−1.4	−1.4	−17.6
SR ZORA-4	−15.225	0.0	1.1	0.8	0.8	−15.2
QSR ZORA	−16.302	−0.1	−1.4	−2.6		
QSR ZORA-4	−15.773	0.0	−1.0	−2.0		
QSR DIRAC	−15.782					

We note in Table III that the EFG in neutral I, which is dominated by the hole in the $5p$-shell, is much smaller than that of the $5p$-orbital of the highly charged hydrogenic Xe^{53+} as given in Tables I and II. The differences in the first column of Table III between the numerically calculated QSR ZORA and SR ZORA results for the neutral iodine closely resemble the differences in the hydrogen-like case, cf. Table II vs. Table I. Again the QSR ZORA results are slightly larger than the SR ZORA results, whereas the effect of the small component is larger in the SR ZORA case than in the QSR ZORA case. Note that in this case the numerically calculated ZORA-4 result agrees within 0.1% with the numerical Dirac result.

In Table III the numerically calculated EFGs are also compared with results from basis set calculations that were obtained with an atomic basis set program. The main difference between the molecular basis set program ADF and this atomic basis set program is that for the evaluation of the Coulomb potential in ADF an auxiliary basis set is used for the fitting of the charge density. The atomic and molecular basis set programs give results within 0.1% of each other. This difference gives an estimate of the accuracy of the numerical integration and charge fitting procedure used in the ADF program.

Table III shows that basis set *A* gives very small basis set errors. Results from this basis set will therefore be used as benchmark values in molecular calculations, where fully numerical calculations are not available. Basis set *B*, which lacks some of the tight $2p$ STOs compared to basis set *A*, still gives very accurate nonrelativistic results, but is less

TABLE IV. Basis set effects on the calculated EFGs at the iodine nucleus. The frozen core approximation is applied in columns *D* and *E*. The differences of the results for a given basis set (frozen core) with respect to the all-electron large basis set *A* results are given in percentage of the basis set *A* results. See text for description of basis sets.

	NR		SR ZORA				ZORA	
	B	*C*	*B*	*C*	*D*	*E*	*B*	*C*
HI	0.0	3.6	−0.6	0.1	−5.8	−24.1	−1.3	−0.9
I_2	0.0	4.1	−0.5	1.8	−5.0	−20.6	−1.1	0.6
IBr	0.0	2.3	−0.6	−0.5	−6.8	−22.8	−1.2	−1.5
ICI	0.0	1.0	−0.6	−1.2	−7.2	−23.4	−1.1	−2.1
IF	0.0	0.5	−0.6	−1.5	−6.8	−22.6	−1.1	−2.3

TABLE V. Effects of small component density (picture-change correction) on the calculated EFGs at the iodine nucleus, defined as the difference between the (SR) ZORA-4 and the (SR) ZORA results, for different basis sets in percentage of the (SR) ZORA result.

	SR ZORA-4					ZORA-4		
	A	*B*	*C*	*D*	*E*	*A*	*B*	*C*
HI	−4.8	−3.2	−2.6	−2.6	−1.9	−2.9	−2.5	−2.3
I_2	−4.8	−3.2	−2.7	−2.6	−1.9	−2.8	−2.5	−2.2
IBr	−4.8	−3.3	−2.7	−2.7	−2.0	−2.7	−2.4	−2.2
ICI	−4.9	−3.3	−2.7	−2.7	−2.0	−2.7	−2.4	−2.1
IF	−4.9	−3.3	−2.7	−2.7	−2.0	−2.8	−2.4	−2.2

accurate in the relativistic case. This can be understood if we look at the radial behavior of a *p*-orbital near the origin[35] (the Dirac large component is denoted ϕ^D),

$$\begin{aligned} &\Psi^{\mathrm{NR}} \sim r^1, \\ &\phi^{\mathrm{SR}}, \Psi^{\mathrm{ZORA}}_{\mathrm{SR}} \sim r^{\sqrt{3-(z^2/c^2)}-1}, \\ &\phi^D, \Psi^{\mathrm{ZORA}}(p_{1/2}) \sim r^{\sqrt{1-(z^2/c^2)}-1}, \\ &\phi^D, \Psi^{\mathrm{ZORA}}(p_{3/2}) \sim r^{\sqrt{4-(z^2/c^2)}-1}, \end{aligned} \tag{40}$$

which apart from the nonrelativistic case is difficult to describe with integer STOs. For an accurate calculation of the EFG it is necessary to describe this inner part of the orbital accurately, which means that one needs a large STO basis set, like for example basis set *A*. On the other hand, if one is satisfied already with an accuracy of a few percent one can also use the much smaller standard ADF all-electron basis set *C*, which does not perform much worse than the larger basis sets *B* and *A*.

A preliminary test of the accuracy of the frozen core approximation is carried out in the SR ZORA case in calculations with basis sets *D* and *E*. In this case the all-electron basis set *C* and the frozen core basis set *D* give the same results, since the valence orbitals are calculated in the same basis and only the $5p$ contribution to the EFG is calculated. Direct contributions to the EFG from core polarization do not show up in this table and will be investigated below. Table III shows that basis set *D* which has a double-ζ description of the core wiggles of the $5p$-orbital gives reasonable results, whereas basis set *E* which only has a single-ζ core wiggles description gives large errors (15%–20%). The standard ADF frozen core basis sets which have this single-ζ core wiggles description are not adequate for EFG calculation.

The EFGs of the valence *p*-electrons of the neutral chlorine, bromine, aluminum, gallium, and indium atoms were also calculated with the use of the spin-restricted $X\alpha$ approximation to the exchange-correlation potential with $\alpha = 0.7$. The calculated results that were obtained with the largest basis sets *A* for these atoms agree within a few tenths of a percent with the corresponding fully numerical results. Other atomic DFT calculations can be found in the review of Lindgren and Rosén,[43] for example.

We now turn to molecular calculations. In Tables IV and V the previously mentioned basis sets and the frozen core approximation are further tested in molecular ADF calculations of the EFG at the iodine nucleus in diatomic interhalogens and HI. In Ref. 44 it was observed that replacing the molecular potential by the sum of the potentials of the neutral spherical reference atoms V_{SA} in the ZORA kinetic energy operator is not a severe approximation. This procedure was called the sum of atoms potential approximation (SAPA) and is used in the ADF calculations. This has the advantage that when the ZORA Kohn–Sham equations are solved self-consistently (SCF) using a basis set, one only needs to calculate the ZORA kinetic energy matrix once, instead of in every cycle in the SCF scheme if the full molecular potential is used. In the calculations SAPA is used both for $T[V]$ and for $Q[V]$.

In the molecular calculations the (nonrelativistic) density functionals for the exchange-correlation energy are used: local density functionals (LDA) with generalized gradient correction (GGC) terms added, namely the Becke correction for exchange (Becke88)[19] and the Perdew correction for correlation.[20] The calculations are performed at the experimental geometries.[45]

Table IV shows that in the nonrelativistical case the extra-tight STOs in basis set *A* compared to basis set *B* do not change the results much. In the relativistic case the relative difference between the results of basis set *A* and those of basis set *B* are larger and almost systematic. They are close to the error that was found in Table III for the EFG due to the valence $5p$-orbital of the neutral iodine. The basis set errors of the results with basis set *C* are larger and they are not so systematic. The errors of basis set *C* are larger in the nonrelativistic case, probably due to the fact that the exponents of the STOs were fitted to SR ZORA orbitals, which is important especially for the smaller basis sets.

The errors in the results with the frozen core and basis set *C* (column *D*) are approximately 6%. We may therefore estimate the contribution of core polarization due to the partial $5p$-hole on I at approximately 6% of the valence contribution. This certainly is too large to be neglected, but it is very much smaller than the contribution from a singly occupied core orbital as given in Table I. The small errors that were observed in Table I between the ZORA-4 and Dirac EFGs (3% maximum, for the $2p$) become insignificant if there is so little core polarization. The errors in the frozen core results with the standard frozen core basis set *E* that only contains a single-ζ description of the core wiggles of

the valence orbitals are more than 20%. This is much larger than the ca. 6% error coming from freezing the core. Apparently the single-ζ description of the core wiggles of the valence orbitals in basis set *E* is thoroughly insufficient, at least the double-ζ level of basis set *C* is required. The ZORA results including SO coupling exhibit even for the large basis *B* deviations larger than 1%, so if results of high precision (below 1%) are required, basis *A* is to be recommended.

Table V shows that the effect of the small component density (picture-change correction) for these molecules is an almost systematic lowering of the absolute values of the EFG at the iodine nucleus. As was found in the atomic case the effect of the small component is larger in the SR ZORA case (4.8%) than in the ZORA case including SO coupling (ca. 2.8%). In the atomic case, with only the effect of the $5p$ taken into account (Table III) the effect is close to that in the present molecular case (in fact slightly larger): 5.1% for the SR ZORA case, compared to 4.8% here, and 3.2% for QSR ZORA, to be compared to ca. 2.8% here for the SO ZORA case. Also the reduction in the effect when going to the smaller basis sets as given in Table V is actually close to the similar reduction of the effect in the smaller basis sets that may be deduced from the data given in Table III. If we wish to have a precision in the results of better than 1%, Table V shows that the reduction in the picture-change effect in going from basis *A* to a smaller basis is too large, at least in the SR ZORA case. Remembering that the small components are directly generated by relation (17) from the ZORA wave function Ψ_i, we infer that for an accurate description of the small component density, which is relatively large in the core region, one needs the tight $2p$ STOs present in basis set *A* in order to describe very accurately the core tails of Ψ_i.

The overall conclusion from Tables IV and V is that even a basis set as extended as basis set *B* cannot guarantee precision of better than 1%. We will therefore use the large basis sets *A* throughout.

VI. ELECTRIC FIELD GRADIENTS IN DIATOMIC HALIDES

In Tables VI and VII results are given of calculated nuclear quadrupole coupling constants (NQCC) of some diatomic molecules. The EFG at a certain nucleus in a.u. is converted to the NQCC in MHz by multiplying the calculated EFG (*zz*-component) in a.u. by a factor of 234.9647 and the nuclear quadrupole moment (NQM) of that nucleus in barns ($1\,\text{barn}=10^{-28}\,\text{m}^2$). Thus the calculated NQCC is proportional to the used NQM. The values of the NQM are taken from the literature for ^{35}Cl,[7] ^{27}Al,[9] and ^{69}Ga,[11] and they are fitted for ^{79}Br, ^{127}I, and ^{115}In; see the last part of this section.

In Table VI calculated halogen (Cl, Br, I) nuclear quadrupole coupling constants are given for the hydrogen halides, the interhalogens, and some metal halides, where the metals are Al, Ga, In, Tl, Cu, and Ag. In Table VII calculated metal (Al, Ga, In) nuclear quadrupole coupling constants are given for the metal halides. In both tables calculated values are compared with experimentally observed values.

The tables show that the scalar relativistic effect, defined as the difference between the SR ZORA-4 result and the NR result, in most cases is (much) larger than the spin–orbit effect, defined as the difference between the ZORA-4 result and the SR ZORA-4 result. In Figs. 1 and 2 calculated NR, SR, ZORA-4, and ZORA-4 iodine NQCCs are compared with observed experimental values. For the interhalogens the scalar relativistic effects are around 1% for Cl, 6% for Br, and 14% for I. As was discussed by Pyykkö and Seth,[38] for example, such effects can already be understood if one looks at the scalar relativistic effect on the valence *p*-shells in neutral atomic calculations. For the copper and especially the silver halides the scalar relativistic effects are much larger, ranging up to more than 40% for the EFG at I in AgI. Large (scalar) relativistic effects were also found at F (and at Cu) in CuF by Pernpointner *et al.*[12] in *ab initio* calculations. In these cases it is the copper or silver atom which indirectly causes the large scalar relativistic effects on the EFG at the halogen center. The scalar relativistic effect for the metals in the metal halides is small for Al, around 2% for Ga, and around 7% for In.

We now turn to the effect of spin–orbit coupling (SOC). The discussion of this effect follows the one given in Ref. 42, where the SOC effects on some molecular properties in closed shell molecules were discussed. The spin–orbit interaction is treated as a modification of a scalar relativistic (LS coupled) starting point. The first-order effect of spin–orbit coupling for these closed shell molecules is zero, and there is only a net effect of off-diagonal spin–orbit coupling if there is off-diagonal spin–orbit interaction between occupied and unoccupied orbitals. It is therefore not surprising that the spin–orbit coupling effect on the calculated EFG is often small. There is, however, a large effect in the thallium halides, where the spin–orbit effect increases the calculated EFG, namely 17% for Cl in TlCl, 20% for Br in TlBr, and 25% for I in TlI; see for TlI also Fig. 1. To understand this effect we can look at the molecular bonding and antibonding orbitals coming from the valence atomic *p*-orbitals of the thallium and the halogen. In the scalar relativistic case the bonding molecular σ- and π-orbitals have more halogen character, whereas the unoccupied antibonding σ- and π-orbitals have more thallium character. Due to the off-diagonal spin–orbit coupling some antibonding orbital character will be mixed into the occupied spinors, which will reduce the charge on the halogen. For the EFG the mixing in of the antibonding σ-orbital is more important than the mixing in of the antibonding π-orbital. The antibonding σ-orbital has relatively more halogen character than the antibonding π-orbital and it mixes more strongly with the bonding σ-orbital. As a result the σ-density on the halogen is decreased and the σ-density at the thallium is increased. Thus the spin–orbit coupling increases the σ-hole at the halogen, resulting in a larger EFG at the position of the halogen nucleus.

It is important to use a large enough basis set for the calculation of the effect of spin–orbit coupling. For example, the spin–orbit effect on the EFG at iodine in HI is less than 0.1% if basis set *C* is used, whereas the more precise results in Table VI using the large basis set *A* show a spin–orbit effect of 2.6%.

We do not find a simple general picture to explain the

TABLE VI. Calculated halogen NQCC (MHz) and comparison with experiment. Nuclear quadrupole moments used (Q in barn): $Q(^{35}\mathrm{Cl}) = -0.08165$ (Ref. 7), $Q(^{79}\mathrm{BR}) = 0.30$ (fitted), $Q(^{127}\mathrm{I}) = -0.69$ (fitted).

		NR	SR ZORA	SR ZORA-4	ZORA	ZORA-4	Observed
AlCl	^{35}Cl	−7.967	−8.073	−8.045	−8.075	−8.060	−8.8290[a]
GaCl	^{35}Cl	−12.54	−12.77	−12.72	−12.80	−12.78	−13.20[b]
InCl	^{35}Cl	−13.06	−13.52	−13.47	−13.74	−13.72	−13.3[b]
TlCl	^{35}Cl	−13.41	−14.17	−14.12	−16.58	−16.56	−15.752[b]
CuCl	^{35}Cl	−39.90	−44.13	−43.95	−44.15	−44.02	−32.125[a]
AgCl	^{35}Cl	−36.36	−46.30	−46.12	−46.31	−46.19	−36.441[a]
HCl	^{35}Cl	−67.22	−68.35	−68.07	−68.35	−68.17	−67.4605[c]
ICl	^{35}Cl	−87.59	−89.47	−89.12	−87.25	−87.01	−85.8[c]
BrCl	^{35}Cl	−102.40	−103.96	−103.55	−103.58	−103.30	−102.378[c]
Cl_2	^{35}Cl	−111.29	−112.91	−112.46	−112.90	−112.60	−115.0[c]
ClF	^{35}Cl	−144.63	−146.71	−146.12	−146.69	−146.28	−145.871 82[c]
AlBr	^{79}Br	68.34	74.06	72.77	74.22	73.75	78.7064[d]
GaBr	^{79}Br	94.0	101.5	99.6	101.9	101.1	105.78[b]
InBr	^{79}Br	98.6	107.6	105.6	109.5	108.6	110.38[b]
TlBr	^{79}Br	100.2	110.6	108.5	130.3	129.7	126.061[b]
CuBr	^{79}Br	300.5	352.5	345.6	352.4	348.6	261.17[e]
AgBr	^{79}Br	276.1	369.8	362.7	369.5	365.7	296.82[b]
HBr	^{79}Br	496.2	537.0	526.6	537.8	531.7	532.239 77[c]
IBr	^{79}Br	662.3	716.0	701.9	704.6	696.2	696.85[b]
Br_2	^{79}Br	760.4	818.0	801.9	815.8	806.5	810.0[c]
BrCl	^{79}Br	820.9	883.4	865.9	880.1	870.1	875.078[c]
BrF	^{79}Br	1016.5	1092.1	1070.3	1085.7	1073.2	1086.891 97[c]
AlI	^{127}I	−235.6	−288.7	−275.8	−291.7	−283.9	−307.407[b]
GaI	^{127}I	−289.7	−352.1	−335.7	−355.4	−346.1	−369.35[b]
InI	^{127}I	−306.6	−372.2	−354.8	−380.5	−371.5	−386.4[b]
TlI	^{127}I	−307.7	−374.8	−357.2	−451.6	−445.7	−438.123[b]
CuI	^{127}I	−960	−1255	−1196	−1247	−1215	−938.07[e]
AgI	^{127}I	−888	−1318	−1256	−1307	−1272	−1060.85[b]
HI	^{127}I	−1555	−1880	−1791	−1892	−1838	−1828.059[c]
I_2	^{127}I	−2137	−2561	−2438	−2517	−2446	−2452.5837[c]
IBr	^{127}I	−2403	−2869	−2730	−2812	−2735	−2731.0[c]
ICl	^{127}I	−2566	−3063	−2915	−2981	−2900	−2929.0[c]
IF	^{127}I	−3020	−3599	−3422	−3483	−3386	−3440.748[c]

[a]Reference 50.
[b]Value taken over from Ref. 48.
[c]Value taken over from Ref. 28.
[d]Reference 51.
[e]Value taken over from Ref. 52.

often subtle spin–orbit effects on the calculated EFG in most calculated molecules. On the other hand, our results show a clear difference in the effect of the small component in scalar relativistic calculations and calculations including spin–orbit coupling. The effect of the small component on the calculated NQCC in the SR ZORA case is an almost systematic decrease of approximately 0.4% for Cl, 1.9% for Br, 4.8% for I, 0.2% for Al, 1.5% for Ga, and 4.0% for In. In the ZORA case the effect of the small component on the calculated NQCC is always smaller than in the SR ZORA case, but it is less systematic. For the interhalogens this effect in the ZORA case is approximately 0.3% for Cl, 1.1% for Br, and 2.8% for I, and for the metals in the metal halides the effect is approximately 0.2% for Al, 1.1% for Ga, and 3.0% for In. For iodine we have discussed the differences that exist with respect to the effect of the small component between ZORA and SR ZORA calculations. This was demonstrated for atomic I, and holds similarly for the other atoms.

The effect of the small component on the results in the SR ZORA calculations can be compared with the same effect in spin-free Dirac–Hartree–Fock (SFDHF) calculations by Visscher *et al.*[15] of the hydrogen halides. They calculated an effect of 0.2% for Cl, 1.3% for Br, and 2.8% for I, which is smaller than the effect of the small component in our SR ZORA calculations of the same molecules. They also calculated the effect of spin–orbit coupling on the calculated EFG, which was defined as the difference between the Dirac–Hartree–Fock (DHF) value and the SFDHF value, and found that it decreases the EFG at the halogen center in the hydrogen halides. On the other hand, we find for the same molecules an increase in EFG at the halogen centers due to the spin–orbit effect, which we define as the difference between the ZORA-4 result and the SR ZORA-4 result. The differences may be related to the fact that there is no unique spin-free Dirac equation,[31] which means that there is also no unique effect of spin–orbit coupling. Visscher *et al.*[15] used the spin-free Dirac equation proposed by Dyall,[46] whereas we use the SR ZORA equation, which is a

TABLE VII. Calculated metal NQCC (MHz) and comparison with experiment. Nuclear quadrupole moments used (Q in barn): $Q(^{27}\mathrm{Al})=0.1466$ (Ref. 9), $Q(^{69}\mathrm{Ga})=0.165$ (Ref. 11), $Q(^{115}\mathrm{In})=0.74$ (fitted).

		Nr	SR ZORA	SR ZORA-4	ZORA	ZORA-4	Observed
AlF	^{27}Al	−38.00	−38.23	−38.15	−38.23	−38.16	−37.75[a]
AlCl	^{27}Al	−31.30	−31.44	−31.37	−31.44	−31.38	−30.410[b]
AlBr	^{27}Al	−29.06	−29.00	−28.94	−28.98	−28.93	−28.006[c]
AlI	^{27}Al	−27.09	−26.74	−26.69	−26.62	−26.57	−25.547[a]
GaF	^{69}Ga	−101.72	−106.06	−104.45	−106.29	−105.11	−107.07[a]
GaCl	^{69}Ga	−88.65	−92.37	−91.00	−92.58	−91.60	−92.1[d]
GaBr	^{69}Ga	−84.15	−87.26	−85.98	−87.44	−86.50	−86.68[a]
GaI	^{69}Ga	−79.86	−82.06	−80.82	−81.98	−81.03	−81.29[a]
InF	^{115}In	−650.6	−731.5	−703.1	−741.2	−720.5	−727.127[a]
InCl	^{115}In	−593.6	−667.6	−641.4	−677.3	−657.7	−659.6[a]
InBr	^{115}In	−573.2	−641.9	−616.7	−651.7	−632.3	−634.7[a]
InI	^{115}In	−553.8	−615.6	−590.9	−624.1	−604.2	−607.5[a]

[a]Value taken over from Ref. 48.
[b]Reference 50.
[c]Reference 51.
[d]Value taken over from Ref. 53.

good approximation to the SR Eq. (4) proposed in Refs. 29, 30.

In Figs. 3, 4, and 5 the ZORA-4 calculated NQCCs for ^{35}Cl, ^{79}Br, and ^{127}I are compared with experimentally observed values. The ZORA-4 calculated results for the NQCC of ^{35}Cl of the interhalogens and HCl are in very nice agreement with experiment. The calculated values for AlCl, GaCl, InCl, and TlCl, which are an order-of-magnitude smaller, are relatively less accurate, but they are still in reasonable agreement with experiment; see also Table VI. The results for CuCl and AgCl, on the other hand, are not very accurate. For these molecules the used density functional fails to describe the electric field gradient with sufficient accuracy. Schwerdtfeger *et al.*[18] showed that many of the presently used functionals, with the exception of some hybrid functionals, give poor results for CuCl. They showed that the results are even worse for the calculation of the EFG at the copper nucleus. They also showed that highly correlated *ab initio* calculations can give very accurate results for CuCl.

The ZORA-4 results for ^{79}Br in Fig. 4 and those for ^{127}I in Fig. 5 are not accurate even for the interhalogens if the NQMs given in Ref. 47 are used. On the other hand, these figures show that if different NQMs for ^{79}Br and ^{127}I are chosen than those given in Ref. 47, one can get the same nice agreement with experiment as was found for ^{35}Cl in Fig. 3. For the fitting procedure the calculated EFGs of the interhalogens and the hydrogen halides were compared with experimental NQCCs. The fitted value was rounded to two significant numbers. The ZORA-4 calculated results with these fitted $Q(^{79}\mathrm{Br})=0.30$ barn and $(^{127}\mathrm{I})=-0.69$ barn are now within 2% of experiment for the interhalogens and the hydrogen halides; see also Table VI. They are in reasonable agreement for the aluminum, gallium, indium, and thallium halides. The agreement with experiment is comparable to the

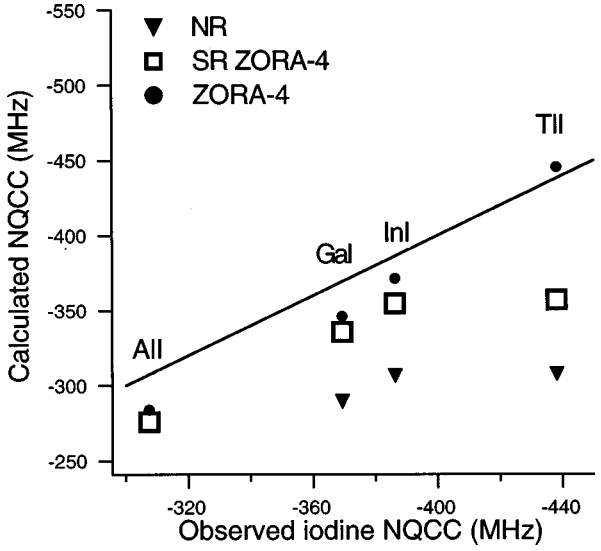

FIG. 1. Nonrelativistic (NR) and (SR) ZORA-4 calculated ^{127}I NQCCs vs. experimentally observed ^{127}I NQCCs. In the calculations the fitted NQM $Q(^{79}\mathrm{I})=-0.69$ barn is used.

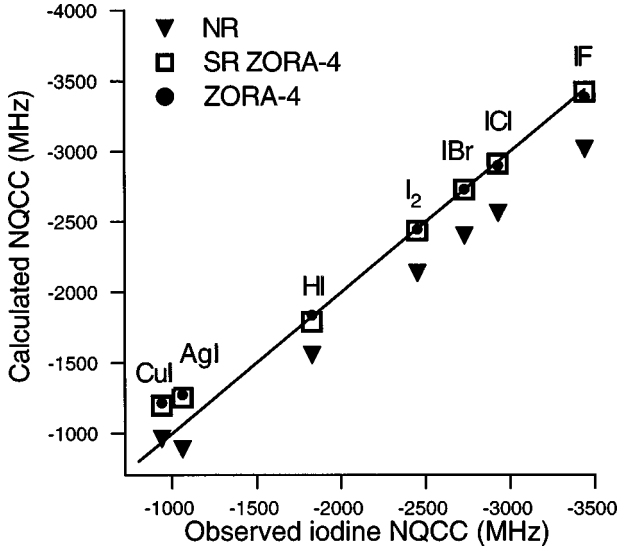

FIG. 2. Nonrelativistic (NR) and (SR) ZORA-4 calculated ^{127}I NQCCs vs. experimentally observed ^{127}I NQCCs. In the calculations the fitted NQM $Q(^{79}\mathrm{I})=-0.69$ barn is used.

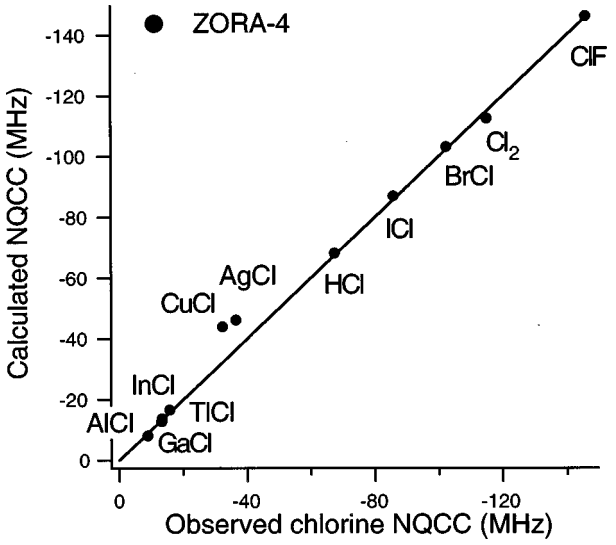

FIG. 3. Calculated ZORA-4 vs. experimentally observed ^{35}Cl NQCCs. Used NQM $Q(^{35}\mathrm{Cl}) = -0.081\,65$ barn (Ref. 7).

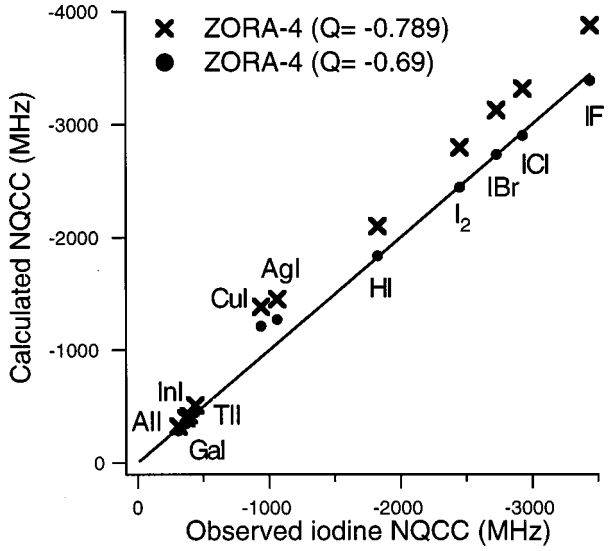

FIG. 5. Calculated ZORA-4 vs. experimentally observed ^{127}I NQCCs. Crosses are calculated with $Q(^{79}\mathrm{I}) = -0.789$ barn (Ref. 47). Dots are calculated with a fitted $Q(^{129}\mathrm{I}) = -0.69$ barn.

one obtained for ^{35}Cl. Again, the copper and silver bromides and the copper and silver iodides are somewhat anomalous.

The ZORA-4 calculated results for ^{27}Al in Table VII are only slightly higher than the experimental values, whereas the ZORA-4 results for ^{69}Ga are only slightly lower than experiment. Note that recently two values for the NQM of ^{69}Ga were recommended, namely $Q(^{69}\mathrm{Ga}) = 0.173$ barn in Ref. 10 and $Q(^{69}\mathrm{Ga}) = 0.165$ barn in Ref. 11. Of the two recommended values for the NQM of gallium, $Q(^{69}\mathrm{Ga}) = 0.165$ barn is more in line with our results, and we have used this value in Table VII. With the fitted $Q(^{115}\mathrm{In}) = 0.74$ barn our ZORA-4 results in Table VII are all in very close agreement with experiment. The ZORA-4 calculated results for ^{115}In would be almost systematically 9% too high if the value of $Q(^{115}\mathrm{In}) = 0.81$, that is listed in Ref. 47, is used.

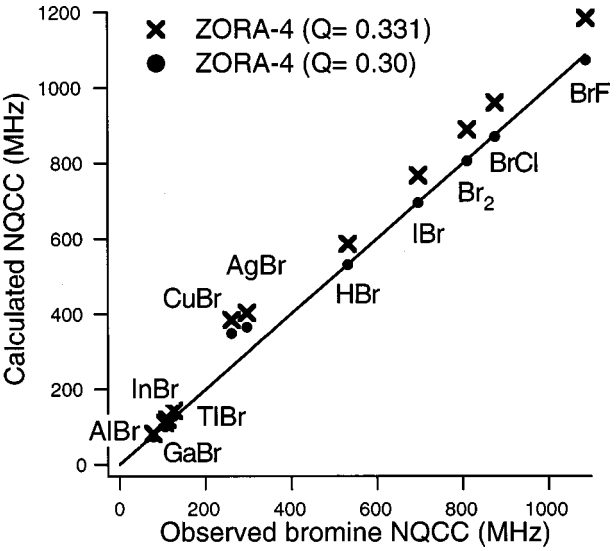

FIG. 4. Calculated ZORA-4 vs. experimentally observed ^{79}Br NQCCs. Crosses are calculated with $Q(^{79}\mathrm{Br}) = 0.331$ barn (Ref. 47). Dots are calculated with a fitted $Q(^{79}\mathrm{Br}) = 0.30$ barn.

Our ZORA-4 DFT calculations suggest that $Q(^{79}\mathrm{Br}) = 0.30(1)$ barn, $Q(^{127}\mathrm{I}) = -0.69(3)$ barn, and $Q(^{115}\mathrm{In}) = 0.74(3)$ barn. These values are based on fitting to the experimental NQCCs using the calculated EFGs. The used molecules in the fitting procedure are the interhalogens and the hydrogen halides for the NQM of ^{79}Br and ^{127}I, and the indium halides for the NQM of ^{115}In. With the use of the fitted NQMs for these molecules the calculated and experimental NQCCs are within 2% of each other. To some extent this gives an idea for the error bars of the fitted NQMs. However, it does not give an estimate for any systematic error. The error bars given are estimated due to several sources of errors. One source is the basis set error, which we believe to be below 1%. A second source of errors is due to the fact that we used a point electric charge and point electric quadrupole for the nucleus instead of a more realistic finite size, and that we did not include vibrational corrections to the calculated nuclear quadrupole coupling constants. We estimate these errors to be in the order of 1%; see also Ref. 48. A different kind of error is due to the used density functional in our calculations. In order to give an estimate for this error we use the fitting procedure also for the evaluation of the NQMs of ^{35}Cl, ^{27}Al, and ^{69}Ga. The selected molecules in this fitting procedure are the interhalogens and hydrogen chloride for the evaluation of the NQM of ^{35}Cl, and the metal halides for the evaluation of the NQMs of ^{27}Al and ^{69}Ga. Note that in our fit we completely neglect the anomalous results for the copper and silver chlorides. The result of the fit gives approximately $Q(^{35}\mathrm{Cl}) = 0.081$ barn, $Q(^{27}\mathrm{Al}) = 0.142$ barn, and $Q(^{69}\mathrm{Ga}) = 0.166$ barn. These fits can be compared with recent values of $Q(^{35}\mathrm{Cl}) = -0.081\,65(80)$ barn,[7] $Q(^{27}\mathrm{Al}) = 0.1466(10)$ barn,[9] $Q(^{69}\mathrm{Ga}) = 0.1650(8)$ barn,[11] and $Q(^{69}\mathrm{Ga}) = 0.173(3)$ barn,[10] that were derived from highly correlated *ab initio* calculations in comparison with results from experiment. These values are only a few percent different from our density functional estimates, which gives us an idea of the accuracy of the used density

functional. Together with the previously mentioned errors, we estimate our total error bars to be approximately 4%.

In agreement with our results *ab initio* correlated Douglas–Kroll calculations[49] suggest a smaller NQM for ^{79}Br and ^{127}I than those given in Ref. 47. However, as was remarked in Ref. 25, picture-change effects may change the recommended NQM values of Ref. 49. It is desirable that future highly correlated *ab initio* relativistic calculations will give us more accurate NQMs of ^{79}Br, ^{127}I, and ^{115}In.

VII. SUMMARY

In this article relativistic effects on electric field gradients have been calculated using the zeroth-order in the regular approximation (ZORA) to the Dirac equation. It has been demonstrated that the proper evaluation of the EFG in the ZORA method requires that the small-components density be taken into account: taking the derivative of the energy with respect to the strength of the nuclear quadrupole field, which is being done numerically in actual applications with various quantum chemical methods[12,11,25,9,10] is equivalent in the ZORA method to using the so-called ZORA-4 density in an expectation value evaluation. Although most of the picture-change correction from a two-component to a four-component formalism is thus covered, this is not yet the case completely. A derivation has been given of the full picture-change correction to order $1/(2c^2-V)$, which demonstrates that the difference with the use of the ZORA-4 density is small.

The intrinsic precision of the ZORA calculations, with full Dirac results as reference, has been investigated in basis set free (fully numerical) atomic calculations. In the case of a one-electron hydrogen-like atom exact relations exist between the results of the calculation of the electric field gradient (EFG) at the nucleus using the ZORA-4 electron density and those using the fully relativistic Dirac electron density. We have considered scalar relativistic as well as quasiscalar relativistic calculations. In the latter that combination of spin–orbit split spinors is taken that would yield an (lm_l) orbital, if those components had identical radial behavior. For valence orbitals the ZORA-4 results are very close to the full Dirac results. It was shown for instance that the ZORA-4 results for the EFG due to a valence p-electron in neutral iodine, represented by the quasiscalar relativistic combination of $p_{1/2}$ and $p_{3/2}$ spinors, were within 0.1% of the fully relativistic (Dirac) results. Deep core orbitals yield somewhat larger differences (for instance 3% for $2p$ in Xe^{53+}). It has been verified that these larger differences for core orbitals are not important since the core contributions to the EFGs are small (in the order of 5% of the valence contribution). This is a consequence of the small polarization of the spherical core densities, as could be demonstrated from comparisons with frozen core calculations. As a further test on the precision of the calculations extensive basis set variations have been carried out. It was shown that it is possible to obtain reasonable EFGs with relatively small basis sets, but in order to get below one percent accuracy very large basis sets are needed. In particular the core wiggles of the valence orbitals need to be described accurately, also in frozen core calculations. A single-ζ representation of the core wiggles for instance leads to large errors (ca. 20%) in the calculated EFGs. The test results taken together demonstrate that the ZORA-4 method in conjunction with a large STO basis set affords an approximation to full Dirac values to within 1%.

Accurate ZORA-4 DFT results employing such a large STO basis set have been obtained for the EFGs at the halogen nuclei in the diatomic interhalogens, the hydrogen halides, and the Al, Ga, In, Tl, Cu, and Ag halides. The (scalar) relativistic effects are almost always too large to be ignored. For the interhalogens they vary from 1% for Cl to 14% for I. They are of course largest at I (for instance 40% in AgI), but even for Cl they can be significant, as in AgCl (27%) or even CuCl (8%). As expected for these closed shell molecules, the effect of spin–orbit coupling is typically much smaller than the scalar relativistic effects. However, it can be significant, as in the thallium halides where it ranges from 17% for TlCl to 25% for TlI.

The calculations suggest that some of the current estimates for the nuclear quadrupole moments need to be adjusted, namely to $Q(^{79}\mathrm{Br})=0.30(1)$ barn, $Q(^{127}\mathrm{I})=-0.69(3)$ barn, and $Q(^{115}\mathrm{In})=0.74(3)$ barn, instead of those given in Ref. 47. The values should be checked by future highly correlated *ab initio* relativistic calculations. With these adjusted NQMs the calculated EFGs at the halogen (Cl, Br, I) centers of the investigated diatomics are in good agreement with experimentally determined NQCCs except for the Cu and Ag halides. This is also true for the calculated EFGs at the metal centers of the metal halides, if the metals are aluminum, gallium, and indium. On the other hand, the calculated EFGs at the halogen centers in the Cu and Ag halides are not in good agreement with experiment, which confirms the results previously found in Ref. 18 for CuCl. Since the discrepancy cannot be due to ''technical'' problems (ZORA, basis sets) it is to be attributed to deficiency of the used density functional: LDA plus gradient corrections due to Becke (Becke88)[19] and Perdew.[20] On the other hand, this functional does give reasonable results for the calculated EFGs in all the other discussed diatomics. One may hope that improved density functionals may remedy the situation for the copper and silver halides, without worsening the results for the other halides.

[1] E. van Lenthe, A. van der Avoird, and P. E. S. Wormer, J. Chem. Phys. **108**, 4783 (1998).
[2] J. E. Harriman, *Theoretical Foundations of Electron Spin Resonance* (Academic, New York, 1978).
[3] Ch. Chang, M. Pelissier, and Ph. Durand, Phys. Scr. **34**, 394 (1986).
[4] J.-L. Heully, I. Lindgren, E. Lindroth, S. Lundqvist, and A.-M. Mårtensson-Pendrill, J. Phys. B **19**, 2799 (1986).
[5] E. van Lenthe, E. J. Baerends, and J. G. Snijders, J. Chem. Phys. **99**, 4597 (1993).
[6] P. Pyykkö, Z. Naturforsch. A **47**, 189 (1992).
[7] D. Sundholm and J. Olsen, J. Chem. Phys. **98**, 7152 (1993).
[8] V. Kellö and A. J. Sadlej, Mol. Phys. **96**, 275 (1999).
[9] V. Kellö, A. J. Sadlej, P. Pyykkö, D. Sundholm, and M. Tokman, Chem. Phys. Lett. **304**, 414 (1999).
[10] M. Tokman, D. Sundholm, and P. Pyykkö, Chem. Phys. Lett. **291**, 414 (1998).
[11] M. Pernpointner and P. Schwerdtfeger, Chem. Phys. Lett. **295**, 347 (1998).
[12] M. Pernpointner, M. Seth, and P. Schwerdtfeger, J. Chem. Phys. **108**, 6722 (1998).
[13] M. Douglas and N. M. Kroll, Ann. Phys. (N.Y.) **82**, 89 (1974).

[14] B. A. Hess, Phys. Rev. A **33**, 3742 (1986).
[15] L. Visscher, T. Enevoldsen, T. Saue, and J. Oddershede, J. Chem. Phys. **109**, 9677 (1998).
[16] W. A. de Jong, L. Visscher, and W. C. Nieuwpoort, J. Mol. Struct. **458**, 41 (1999).
[17] P. Dufek, P. Blaha, and K. Schwarz, Phys. Rev. Lett. **75**, 3545 (1998).
[18] P. Schwerdtfeger, M. Pernpointner, and J. K. Laerdahl, J. Chem. Phys. **111**, 3357 (1999).
[19] A. D. Becke, Phys. Rev. A **38**, 3098 (1988).
[20] J. P. Perdew and Y. Wang, Phys. Rev. B **33**, 8800 (1986).
[21] R. H. Havlin, N. Godbout, R. Salzmann, M. Wojdelski, W. Arnod, C. E. Schulz, and E. Oldfield, J. Am. Chem. Soc. **120**, 3144 (1998).
[22] N. Godbout, R. Havlin, R. Salzmann, P. G. Debrunner, and E. Oldfield, J. Phys. Chem. A **102**, 2342 (1998).
[23] L. A. Eriksson, O. L. Malkina, V. G. Malkin, and D. R. Salahub, Int. J. Quantum Chem. **63**, 575 (1997).
[24] E. J. Baerends, W. H. E. Schwarz, P. Schwerdtfeger, and J. G. Snijders, J. Phys. B **23**, 3225 (1990).
[25] V. Kellö and A. J. Sadlej, Int. J. Quantum Chem. **68**, 159 (1998).
[26] M. H. Palmer and J. A. Blair-Fish, Z. Naturforsch. A **53**, 370 (1998).
[27] M. H. Palmer, J. A. Blair-Fish, P. Sherwood, and M. F. Guest, Z. Naturforsch. A **53A**, 383 (1998).
[28] M. H. Palmer, Z. Naturforsch. A **53**, 615 (1998).
[29] H. Gollisch and L. Fritsche, Phys. Status Solidi B **86**, 145 (1978).
[30] D. D. Koelling and B. N. Harmon, J. Phys. C **10**, 3107 (1977).
[31] L. Visscher and E. van Lenthe, Chem. Phys. Lett. **306**, 357 (1999).
[32] E. van Lenthe, E. J. Baerends, and J. G. Snijders, J. Chem. Phys. **101**, 9783 (1994).
[33] A. J. Sadlej, J. G. Snijders, E. van Lenthe, and E. J. Baerends, J. Chem. Phys. **102**, 1758 (1995).
[34] E. van Lenthe, E. J. Baerends, and J. G. Snijders, Chem. Phys. Lett. **236**, 235 (1995).
[35] R. van Leeuwen, E. van Lenthe, E. J. Baerends, and J. G. Snijders, J. Chem. Phys. **101**, 1272 (1994).
[36] K. G. Dyall and E. van Lenthe, J. Chem. Phys. **111**, 1366 (1999).
[37] L. L. Foldy and S. A. Wouthuysen, Phys. Rev. **78**, 29 (1950).
[38] P. Pyykkö and M. Seth, Theor. Chem. Acc. **96**, 92 (1997).
[39] E. J. Baerends, D. E. Ellis, and P. Ros, Chem. Phys. **2**, 42 (1973).
[40] G. te Velde and E. J. Baerends, J. Comput. Phys. **99**, 84 (1992).
[41] C. Fonseca Guerra, O. Visser, J. G. Snijders, G. te Velde, and E. J. Baerends, in *Methods and Techniques in Computational Chemistry*, edited by E. Clementi and G. Corongiu (STEF, Cagliari, 1995), Chap. 8.
[42] E. van Lenthe, J. G. Snijders, and E. J. Baerends, J. Chem. Phys. **105**, 6505 (1996).
[43] I. Lindgren and A. Rosén, Case Stud. At. Phys. **4**, 93 (1974).
[44] P. H. T. Philipsen, E. van Lenthe, J. G. Snijders, and E. J. Baerends, Phys. Rev. B **56**, 13556 (1997).
[45] M. E. Radzig and B. M. Smirnov, *Reference Data on Atoms, Molecules, and Ions* (Springer-Verlag, Berlin, 1985).
[46] K. G. Dyall, J. Chem. Phys. **100**, 2118 (1994).
[47] *Handbook of Chemistry and Physics*, 75th ed., edited by D. R. Lide (CRC, Boca Raton, 1994).
[48] E. A. C. Lucken, in *Advances in Nuclear Quadrupole Resonance*, edited by J. A. S. Smith (Wiley, New York, 1983), Vol. 5.
[49] V. Kellö and A. J. Sadlej, Mol. Phys. **89**, 127 (1996).
[50] K. D. Hensel, C. Styger, W. Jäger, A. J. Merer, and M. C. L. Gerry, J. Chem. Phys. **99**, 3320 (1993).
[51] K. A. Walker and M. C. L. Gerry, J. Mol. Spectrosc. **193**, 224 (1999).
[52] J. Sheridan, in *Advances in Nuclear Quadrupole Resonance*, edited by J. A. S. Smith (Wiley, New York, 1983), Vol. 5.
[53] W. Gordy and R. L. Cook, *Microwave Molecular Spectra* (Wiley, New York, 1984).